Eur. Phys. J. C 39, 451–464 (2005)
Digital Object Identifier (DOI) 10.1140/epjc/s2004-02098-5

THE EUROPEAN PHYSICAL JOURNAL C

Jet production in pA and AA collisions in the perturbative QCD pomeron model

M.A. Braun[a]

Department of High Energy Physics, University of S. Petersburg, 198504 S. Petersburg, Russia

Received: 12 October 2004 / Revised version: 22 November 2004 /
Published online: 21 January 2005 –

Abstract. Inclusive cross-sections for gluon jet production are studied numerically in the perturbative QCD pomeron model for pA and central AA collisions at high energies. Two forms for the inclusive cross-sections, with and without emission from the triple pomeron vertex, are compared. The difference was found to reduce to a numerical factor $\sim 0.7 \div 0.8$ for momenta below the saturation momentum $Q_{\rm s}$. Above $Q_{\rm s}$ no difference was found at all. For pA collisions the gluon spectrum was found to be $\sim A^{0.7}$ at momenta k below $Q_{\rm s}$ and $\sim A^{0.9}$ above it. For central AA collisions it was found to be $\sim A$ at momenta k below $Q_{\rm s}$ and $\sim A^{1.1}$ above it. At large k the spectrum goes like $1/k^{2.7\div 3.3}$, flattening with energy. The multiplicities turned out to be proportional to $A^{0.7}$ for pA collisions and A for central AA collisions with a good precision. In the latter case they are becoming more peaked at the center with the growth of energy. Their absolute values are high and grow rapidly with energy in accordance with the high value of the BFKL intercept.

1 Introduction

New experimental data on heavy-ion collisions at RHIC and the prospect of such data to be obtained at LHC in the future made the spectra of produced secondaries and in particular their dependence on the atomic number of colliding nuclei attract much attention. One would like to have relevant predictions based on the fundamental theory and not purely phenomenological. At present the only candidate for this is the hard pomeron model derived from perturbative QCD. Originally constructed for the description of high-energy low-x hadronic scattering (the BFKL model [1]) it has subsequently been generalized to hadronic or deep inelastic scattering on nuclei [2,3] and nucleus–nucleus scattering [4]. The model suffers from a serious drawback related to the use of a fixed and not running strong coupling constant. Curing it does not look too promising, since due to the absence of ordering of momenta in the model, it also means solving the confinement problem. However in spite of this defect the model seems to describe high-energy phenomena in a qualitatively reasonable manner. Also, attempts to include the running of the coupling in some effective way have shown that the effect of the running is not at all overwhelming, although this introduces some quantitative changes into the predictions. So, also for lack of something better, the perturbative QCD pomeron model appears to give a reasonable basis for the discussion of particle production in very high-energy heavy-ion collisions. Of course due to the perturbative character of the model it can only give predictions for the production of jets, leaving jet-to-hadrons conversion to the non-perturbative fragmentation mechanism. Also it has to be stressed that the model is, by construction, oriented towards very high (asymptotic) energies or, equivalently, very low values of x. So its application to present-day energies does not seem to be fully justified, at least in the lowest order of perturbation expansion to be used in the present calculations. This has to be kept in mind when comparing the prediction of the model with the existing experimental data.

From the start it has to be noted that in the model scattering amplitudes can be found comparatively easily only for hadron–nucleus collisions. They are given by a set of all pomeron fan diagrams, which are summed by the non-linear evolution equation of [2,3]. Nucleus–nucleus collision amplitudes are described in the model by complicated equations, whose solution is quite difficult to obtain even numerically (see [5] for partial results). Happily, as was shown in [6], due to Abramovsky–Gribov–Kancheli (AGK) cancellations [7], to find the single inclusive distributions one does not have to solve these equations, but only to sum the appropriate sets of fan diagrams, that is to solve the much simpler hadron–nucleus problem. Still the latter problem involves a numerical study of considerable complexity. So up to now there has been no consistent calculation of the jet spectra for realistic nuclei at very high energies, although some preliminary attempts has been made in [8–11]. In all cases however the authors relied on very drastic simplifications, from the start choosing for the nuclear structure and/or for the gluon distributions in the colliding nuclei some primitive explicit forms in accordance with their own tastes and prejudices. In fact these forms appear to be rather far

[a] e-mail: mijail@fpaxpl.usc.es

from the realistic ones, which correspond to actual participants and follow from the calculations. This gave us the motivation to calculate numerically the jet spectra in hadron–nucleus and nucleus–nucleus collisions as predicted by the hard pomeron model in a consistent manner.

Another goal of the present calculations has been to compare the results obtained on the basis of the expression for the inclusive cross-section which follows from the AGK rules applied to the diagrams with QCD pomerons interacting via the three-pomeron coupling [6] with a somewhat different expression obtained from the color dipole picture [12]. Our calculations show that these two formally different expressions lead to completely identical results at momenta of the order of or higher than the value of the so-called saturation momentum $Q_{\rm s}$. At momenta substantially lower than $Q_{\rm s}$ the color dipole cross-sections differ from the ones from the AGK rules by a universal constant factor $\sim 0.7 \div 0.8$.

In both cases the A-dependence of the spectra at momenta below $Q_{\rm s}$ is found to be suppressed as compared to the naive probabilistic expectations, which predict that it should follow the number of binary collisions, $\propto A$ for pA scattering and $\propto A^{4/3}$ for AA scattering at fixed impact parameter. Instead we have found a behavior damped by roughly a factor $A^{1/3}$, that is $\propto A^{0.7}$ for pA collisions and $\propto A$ for central AA collisions. Since $Q_{\rm s}$ grows with energy very fast, the region where the spectra behave in this manner extends with energy to include all momenta of interest. At momenta greater than $Q_{\rm s}$ the spectra grow faster but still much slowlier than the number of binary collisions (a numerical fit gives something like $\propto A^{1.1}$ for central AA collisions).

Note that in the last years a few more phenomenologically oriented studies of particle production in nucleus–nucleus production at very high energies have been presented, in the framework of the color-condensate model [13] solved in the classical approximation on the lattice [10] and in the saturation model [11]. In both approaches the quantum evolution of the nuclear gluon density was neglected and the saturation momentum was introduced as a parameter fitted to the experimental data at RHIC. Although some of their predictions (proportionality of the multiplicity to A modulo logarithms) agree with our calculations with full quantum evolutions, the quantitative results are rather different. We postpone a more detailed discussion of this point until the section with our conclusions.

The results of this study continue and extend the ones published in [14]. As compared to that publication we explore the y-dependence of the cross-sections and, apart from AA central collisions, study pA collisions as well. We also concentrate on energies accessible in the near future (at LHC) to be closer to the experimental situation. Still we have to stress that our results do not pretend to describe the existing data obtained at RHIC. As mentioned, the perturbative QCD pomeron model studies phenomena at very high energies, at which the coupling constant becomes sufficiently small. The characteristic energetic variable for the model is the scaled rapidity $\bar{Y} = (N_c\alpha_{\rm s}/\pi)Y$. One observes that the solution of the non-linear evolution equation acquires its standard scaling form, independent of the choice of the initial conditions, at $\bar{Y} > 1.5 \div 2$. With $\alpha_{\rm s} \sim 0.2$ this sets the lower limit for the rapidity at the center, at which our results can be applied, to be $7.5 \div 10$, which implies the overall rapidity for the collision in the region $15 \div 20$. This is much higher than the rapidities at RHIC but well within the possibilities of LHC. So we may hope that our predictions can be tested at LHC, but we have little chance of success for the data from RHIC. In relation to the latter the model can possibly indicate some trends of the observable cross-sections with the growth of energy, much in the same manner as it predicted the growth of the total cross-sections with energy at the time of its appearance (although the rate of this growth was grossly overestimated). The proportionality of the spectra to the number of participants and not to the number of binary collisions that was found well agrees with the experimental findings and is one of these trends.

2 Basic equations

2.1 Total cross-sections

As mentioned in the Introduction, the scattering amplitude can be relatively easily found for hA collisions but not for AB collisions. Correspondingly here we present formulas which serve to calculate the total cross-sections for hadron (proton)–nucleus collisions. This cross-section is given by an integral over the impact parameter b and the pomeron transverse dimension r as follows:

$$\sigma_A(y) = 2\int {\rm d}^2b{\rm d}^2r\rho(r)\Phi(y,r,b). \tag{1}$$

Here y is the overall rapidity, $\rho(r)$ is the color dipole density of the projectile (proton) and $\Phi(y,r,b)$ is the color dipole–nucleus cross-section at fixed y, r and b, given by the sum of all fan diagrams stretched between the projectile and nucleus.

The function $\phi(y,r,b) = \Phi(y,r,b)/(2\pi r^2)$, in the momentum space, satisfies the well-known non-linear equation [2,3]

$$\frac{\partial\phi(y,q,b)}{\partial\bar{y}} = -H\phi(y,q,b) - \phi^2(y,q,b), \tag{2}$$

where $\bar{y} = \bar{\alpha}y$, $\bar{\alpha} = \alpha_{\rm s}N_c/\pi$, $\alpha_{\rm s}$ and N_c are the strong coupling constant and the number of colors, respectively, and H is the BFKL Hamiltonian. Equation (2) has to be solved with an initial condition at $y = 0$. For the heavy nucleus at rest it is determined by the color dipole distribution in the proton smeared by the profile function of the nucleus. In our calculations we take this distribution in accordance with the Golec-Biernat distribution [15], duly generalized for the nucleus:

$$\phi(0,q,b) = \frac{1}{2}AT_A(b)\sigma_0 f(q), \tag{3}$$

where

$$f(q) = -\frac{1}{2}{\rm Ei}(-x), \quad x = \frac{q^2}{0.218\,{\rm GeV}^2}, \tag{4}$$

$\sigma_0 = 20.8\,\mathrm{mb}$ and $T_A(b)$ is the standard nuclear profile function, which we have taken from the Woods–Saxon nuclear density.

To write the final formula for the cross-section we have to find the dipole distribution $\rho(r)$ in the incoming proton, consistent with the initial condition (3). To this end we use the expression for the initial condition in terms of $\rho(r)$ [3]:

$$\Phi(0,r,b) = \frac{1}{2} A T_A(b) g_0^4 \nabla^{-4} \rho(r), \tag{5}$$

where g_0 is the strong coupling constant at a very low scale determined by the intrinsic momenta inside the proton. This translates into the relation in the momentum space:

$$\rho(q) = -\frac{2\pi\sigma_0}{g_0^4} f_2(q), \quad f_2(q) = \left(\frac{\mathrm{d}}{\mathrm{d}\ln q}\right)^2 f(q). \tag{6}$$

We also introduce the gluon density function

$$h(y,q,b) = q^2\nabla_q^2\phi(y,q,b) = \left(\frac{\mathrm{d}}{\mathrm{d}\ln q}\right)^2 \phi(y,q,b) \tag{7}$$

to finally obtain

$$\sigma_A(y) = \frac{\sigma_0}{8\pi^2\alpha_{\mathrm{s}0}^2} \int \mathrm{d}^2b\mathrm{d}^2q f_2(q) h(y,q,b), \tag{8}$$

where $\alpha_{\mathrm{s}0} = g_0^2/(4\pi)$ refers to the scale inside the proton. Of course the structure of the proton is non-perturbative, so that $\alpha_{\mathrm{s}0}$ emerges as a new parameter in the model related to hadronic processes.

Note that with these normalizations the cross-section at $y = 0$ corresponds to a pure double gluon exchange. A better approximation consists in using an eikonalized ansatz for the initial condition:

$$\Phi(0,r,b) \to 1 - \mathrm{e}^{-\Phi(0,r,b)}. \tag{9}$$

From the formal point of view this implies including higher orders in $1/N_c^2$ and so cannot be justified. Also, as follows from the calculations, already at $\bar{y} = 1$ the eikonalization becomes forgotten and the results with eikonalized and non-eikonalized initial conditions are practically the same. Still at $y = 0$ they are different and the cross-section without eikonalization is found to be unreasonably large. For this reason we use the eikonalized initial condition for the total hA cross-sections at low y and the non-eikonalized one elsewhere.

2.2 Inclusive cross-sections and multiplicities

In the study of inclusive cross-sections we have to distinguish the overall rapidity of the collision Y and the rapidity of the produced particle y. Our basic quantities will be the inclusive cross-sections $I_A(y,k)$ and $I_{AB}(y,k)$ to produce a jet with the transverse momentum k at rapidity y in a collision of a proton off a nucleus with the atomic number A or two nuclei with atomic numbers A and B:

$$I_{A(B)}(y,k) = \frac{(2\pi)^2 \mathrm{d}\sigma_{A(B)}}{\mathrm{d}y\mathrm{d}^2k}. \tag{10}$$

Both cross-sections can be represented as an integral over the impact parameter b:

$$I_{A(B)}(y,k) = \int \mathrm{d}^2b I_{A(B)}(y,k,b). \tag{11}$$

We shall study the pA cross-section as it stands, but for the nucleus–nucleus case our study will be restricted to the inclusive cross-sections at a fixed impact parameter $b = 0$ (central collisions) and identical nuclei, $A = B$. To simplify notation we shall denote the AA cross-sections also as I_A in all places where it cannot lead to confusion. The corresponding multiplicities at a fixed rapidity y will be given by

$$\mu_A(y) = \frac{1}{\sigma_A} \int \frac{\mathrm{d}^2k}{(2\pi)^2} I_A(y,k) \tag{12}$$

for the pA case and

$$\mu_{AA}(y) = \frac{1}{\sigma_{AA}(b=0)} \int \frac{\mathrm{d}^2k}{(2\pi)^2} I_{AA}(y,k,b=0), \tag{13}$$

for the AA case, where σ_A and $\sigma_{AA}(b)$ are the total inelastic cross-sections for the pA collision and for the collision of two identical nuclei at the fixed impact parameter b. For heavy nuclei one expects that $\sigma_A(b=0) \simeq 1$, so that the multiplicity (13) is just the integral of the inclusive cross-section over momenta.

As argued in [4], in the perturbative QCD with a large number of colors the nucleus–nucleus interaction is described by a set of tree diagrams constructed with BFKL pomeron Green functions and triple pomeron vertices for their splitting and fusing. The structure of the interaction at the vertex is illustrated in Fig. 1, in which horizontal lines correspond to real gluons produced in the intermediate states and vertical and inclined lines describe propagating reggeized gluons. From this structure one sees that the produced gluons are contained in the intermediate states of the interacting pomerons, so that to get the inclusive cross-section one has to "open" these pomerons, that is to fix the momentum of one of the intermediate real gluons in them. For pA collisions this leaves the diagrams of the type shown in Fig. 2a. For the nucleus–nucleus case a similar

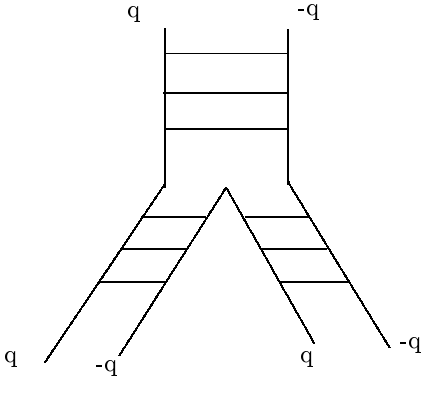

Fig. 1. Interaction of three BFKL pomerons at the splitting vertex

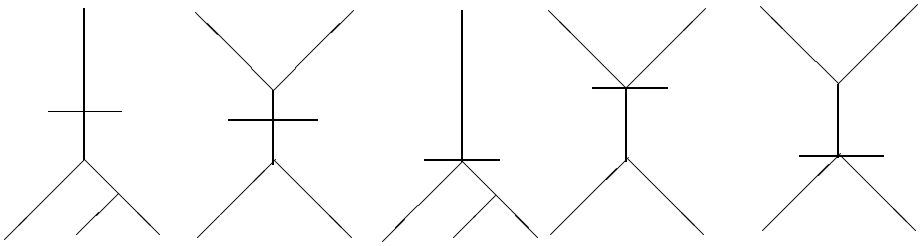

Fig. 2a–e. Typical diagrams for the inclusive cross-section in nucleus–nucleus collisions

production mechanism in the old-fashioned local pomeron model was proven to lead to inclusive cross-sections given by a convolution of two sets of fan diagrams connecting the emitted particle to the two nuclei times the vertex for the emission (Fig. 2b). The proof was based on the AGK rules appropriately adjusted for the triple pomeron interaction [16]. It was later shown in [17] that the AGK rules are fulfilled for interacting BFKL pomerons. So the same arguments as in [16] allow one to demonstrate that for collisions of two nuclei the inclusive cross-section will be given by the same Fig. 2b, that is, apart from the emission vertex, by the convolution of two sums of fan diagrams, constructed of BFKL pomerons and triple pomeron vertices, propagating from the emitted particle towards the two nuclei [6].

Taking into account the form of the emission vertex [6] we obtain for the pA case

$$I_A(y,k) = \frac{8N_c\alpha_s}{k^2}\int \mathrm{d}^2\beta\mathrm{d}^2r\mathrm{e}^{\mathrm{i}kr}\Delta\Psi(Y-y,r)\cdot\Delta\Phi(y,r,\beta), \tag{14}$$

and for the AA case at $b=0$[1]

$$I_{AA}(y,k) = \frac{N_c\alpha_s}{\pi^2\alpha_{s0}^2k^2}\int \mathrm{d}^2\beta\mathrm{d}^2r\mathrm{e}^{\mathrm{i}kr}\Delta\Phi(Y-y,r,\beta)\cdot\Delta\Phi(y,r,\beta). \tag{15}$$

Here $\Psi(y,r)$ is a pomeron at rapidity y and of the transverse dimension r coupled to the incoming proton. Its normalization at $y=0$ is

$$\Psi(0,r) = \frac{2\Phi(0,r,b)}{g_0^4AT_A(b)} \tag{16}$$

(obviously the right-hand side of (16) does not depend on b). The Δ's are two-dimensional Laplacians applied to the Ψ and Φ's.

Later from the color dipole formalism a slightly different form for the inclusive cross-section was derived in [12]. For the dipole–nucleus scattering case it corresponds to changing

$$2\Phi(y,\beta,r) \to 2\Phi(y,\beta,r) - \Phi^2(y,\beta,r). \tag{17}$$

Note that in [12] it was stated that the change was from the "quark dipole" Φ to the "gluon dipole" $2\Phi-\Phi^2$. As seen from (17) it is not. In fact the change is from two quark dipoles to a gluon one: $2\Phi\to 2\Phi-\Phi^2$. This is equivalent to adding to the AGK contribution (15) a new one which has the meaning of the emission of the gluon from the triple pomeron vertex itself. Such a contribution is not prohibited in principle. From our point of view, taking into account the structure of the vertex shown in Fig. 1, its appearance is difficult to understand. However in this paper we do not pretend to discuss the validity of the two proposed formulas for the inclusive cross-sections on the fundamental level, leaving this question for later studies. Rather we shall compare the cross-sections which follow from them after numerical calculations.

For the pA case this recipe implies taking into account a new diagram shown in Fig. 2c. As a result, one finds, instead of (14), the Kovchegov–Tuchin (KT) cross-section

$$I_A^{\mathrm{KT}}(y,k) = \frac{4N_c\alpha_s}{k^2} \times\int \mathrm{d}^2\beta\mathrm{d}^2r\mathrm{e}^{\mathrm{i}kr} \times\Delta\Psi(Y-y,r)\cdot\Delta[2\Phi(y,r,\beta)-\Phi^2(y,r,\beta)]. \tag{18}$$

For the nucleus–nucleus case the recipe of [12] implies taking into account the two new diagrams for the inclusive cross-sections shown in Fig. 2d,e. The nucleus–nucleus cross-section thus becomes

$$I_{AA}^{\mathrm{KT}}(y,k) = \frac{N_c\alpha_s}{2\pi^2\alpha_{s0}^2k^2} \times\int \mathrm{d}^2\beta\mathrm{d}^2r\mathrm{e}^{\mathrm{i}kr}\left[2\Delta\Phi(Y-y,r,\beta)\Delta\Phi(y,r,\beta) -\Delta\Phi(Y-y,r,\beta)\Delta\Phi^2(y,r,\beta) -\Delta\Phi^2(Y-y,r,\beta)\Delta\Phi(y,r,\beta)\right]. \tag{19}$$

Passing in our formulas to the momentum space we find (suppressing the dependence on y and β)

$$\Delta\Phi(r)\to 2\pi q^2\Delta_q\phi(q)\equiv 2\pi h(q). \tag{20}$$

Introducing also a function similar to h for the pomeron Ψ:

$$\Delta\Psi(r) = 2\pi h^{(0)}(q) \tag{21}$$

we can express the cross-sections (14) and (15) via the gluon distributions $h^{(0)}(q)$ and $h(q)$ in a factorized form:

$$I_A(y,k) = \frac{8N_c\alpha_s}{k^2}\int \mathrm{d}^2\beta\mathrm{d}^2qh^{(0)}(Y-y,q)h(y,k-q,\beta), \tag{22}$$

[1] A slightly different coefficient as compared to [14] is due to a different normalization of Φ.

and for the AA case at $b = 0$

$$I_{AA}(y,k) = \frac{N_c\alpha_{\rm s}}{\pi^2\alpha_{\rm s0}^2k^2}\int {\rm d}^2\beta{\rm d}^2q h(Y-y,q,\beta)h(y,k-q,\beta). \tag{23}$$

The KT cross-section contains an additional term

$$X(r) = -\Delta\Phi^2(r) = -\Delta(2\pi)^2r^4\phi^2(r). \tag{24}$$

We transform it to the momentum space:

$$X(q) = q^2\int {\rm d}^2r{\rm e}^{-{\rm i}qr}\Phi^2(r) = (2\pi)^2q^2\int {\rm d}^2r\left(r^2\phi(r)\right)^2. \tag{25}$$

On the other hand

$$r^2\phi(r) = -\int\frac{{\rm d}^2q'}{(2\pi)^2}{\rm e}^{{\rm i}q'r}\Delta'\phi(q'). \tag{26}$$

So we get

$$X(q) = q^2\int {\rm d}^2q_1\Delta\phi(q_1)\cdot\Delta\phi(q-q_1). \tag{27}$$

Taking into account that

$$\Delta\phi(q) = -2\pi\delta(q) + \frac{h(q)}{q^2} \tag{28}$$

gives

$$X = -4\pi h(q) + q^2\int\frac{{\rm d}^2q_1}{q_1^2(q-q_1)^2}h(q_1)h(q-q_1). \tag{29}$$

This should be added to the first term in the 2nd factor of the integrand in (18), which according to (20) is just $4\pi h(q)$. So in the end in the KT cross-section instead of $4\pi h(q)$ will appear the second term in (29). Introducing the function

$$w(q) = \frac{q^2}{2\pi}\int\frac{{\rm d}^2q_1}{q_1^2(q-q_1)^2}h(q_1)h(q-q_1), \tag{30}$$

we finally find that the KT cross-section is obtained from the AGK cross-section by the substitution $h(q)\to w(q)/2$:

$$I_A^{\rm KT}(y,k) = \frac{4N_c\alpha_{\rm s}}{k^2}\int {\rm d}^2\beta{\rm d}^2q h^{(0)}(Y-y,q)w(y,k-q,\beta). \tag{31}$$

Now we pass to the nucleus–nucleus cross-section. For different colliding nuclei the KT rule means (see Fig. 2)

$$\begin{aligned}&2\Delta\Phi_A(r)\cdot\Delta\Phi_B(r)\to\\ &\quad 2\Delta\Phi_A(r)\cdot\Delta\Phi_B(r) - \Delta\Phi_A(r)\cdot\Delta\Phi_B^2(r)\\ &\quad -\Delta\Phi_A^2(r)\cdot\Delta\Phi_B(r)\end{aligned} \tag{32}$$

where we again suppress all other arguments in Φ evident from (19). Going to the momentum space, we have

$$\Delta\Phi(r)\to 2\pi h(q),\quad -\Delta\Phi^2(r)\to -4\pi h(q) + 2\pi w(q), \tag{33}$$

and we shall find the KT cross-section at a given impact parameter β as follows:

$$\begin{aligned}I_{AB}^{\rm KT}(y,k,\beta) &= \frac{N_c\alpha_{\rm s}}{2\pi^2\alpha_{\rm s0}^2k^2}\\ &\times\int {\rm d}^2b{\rm d}^2q\left[h_A(Y-y,q,\beta-b)w_B(y,k-q,b)\right.\\ &+w_A(Y-y,q,\beta-b)h_B(y,k-q,b)\\ &\left.-2h_A(Y-y,q,\beta-b)h_B(y,k-q,b)\right].\end{aligned} \tag{34}$$

For central collisions of identical nuclei at mid-rapidity this simplifies to

$$\begin{aligned}I_{AA}^{\rm KT}(Y/2,k,0) &= \frac{N_c\alpha_{\rm s}}{\pi^2\alpha_{\rm s0}^2k^2}\\ &\times\int {\rm d}^2b{\rm d}^2q h(Y/2,q,b)\\ &\times\left(w(Y/2,k-q,b) - h(Y/2,k-q,b)\right).\end{aligned} \tag{35}$$

So in the end the KT cross-sections can also be expressed via the function $h(q)$.

The function $h(y,k,\beta)$ has the normalization property [6]

$$\int\frac{{\rm d}^2k}{k^2}h(y,k,\beta) = 1 \tag{36}$$

and at sufficiently high y acquires the scaling property

$$h(y,k\beta) = h\left(k/Q_{\rm s}(y,\beta)\right), \tag{37}$$

where $Q_{\rm s}(y,\beta)$ is the above-mentioned saturation momentum. From (36) and (37) one easily establishes some properties of the new function w_A. Obviously it scales with the same saturation momentum when h_A does,

$$w(y,k\beta) = w\left(k/Q_{\rm s}(y,\beta)\right). \tag{38}$$

At $k\to\infty$ it has the asymptotic

$$w(y,k,\beta)_{k\to\infty}\sim 2h(y,k,\beta) \tag{39}$$

and finally

$$\int {\rm d}^2k w(y,k,\beta) = 2\int {\rm d}^2k h(y,k,\beta). \tag{40}$$

These properties immediately allow one to make some preliminary comparisons between the cross-sections given by (22) and (23), on the one hand, and (31) and (34), on the other. Obviously if $k/Q_{\rm s}$ is large both expressions give the same cross-section due to (40). In the opposite limit of small $k/Q_{\rm s}$, the scaling property allows one to conclude that the ratio of the two cross-sections is a universal constant which does not depend on y, nor on A nor on β. Our numerical results confirm these predictions.

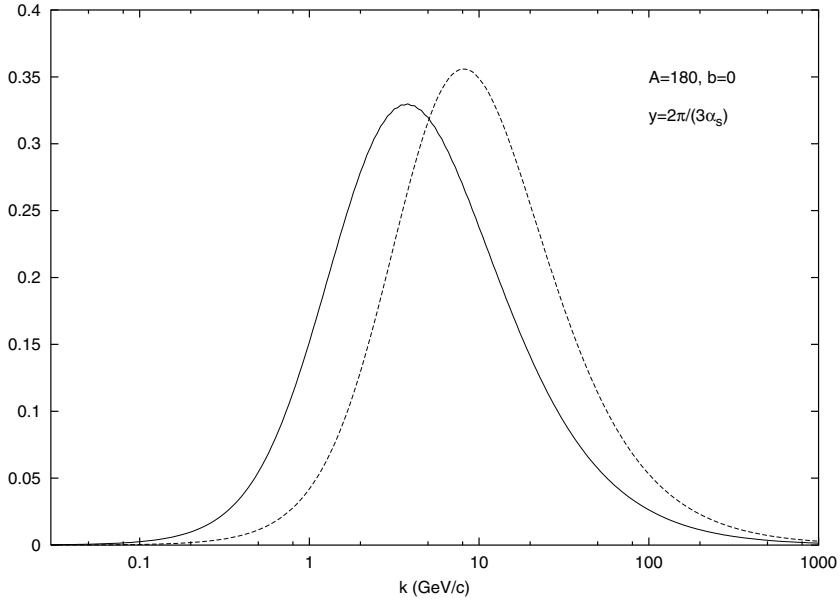

Fig. 3. Gluon densities $h(k)$ (the left curve) and $w(k)$ for $A = 180$ at $b = 0$ and $\bar{y} = 2$

3 Results

Our cross-sections depend on three parameters, σ_0 and two coupling constants α_s at the comparatively large evolution scale and α_{s0} at the very low proton scale. As mentioned, we have a certain control on the value of σ_0 from the experimental data on the proton structure function at low x, embodied in the parametrization (3) borrowed from [15]. However we can have only very general ideas about the possible values for the coupling constant at the two scales involved, since the coupling constant is not running in the model. The common wisdom is to take $\alpha_s = 0.2$, which is considered to be the value reached by the running coupling at relatively low scales. In our calculations we have taken this value for the evolution equation and for the production vertex. However with the same value for α_{s0} we find the total pp and pA cross-sections at low energies to be roughly four times greater than the experimental data. To bring them into the physically reasonable range we have to double the value of α_{s0}. So in our calculations we have taken $\alpha_{s0} = 0.4$.

3.1 The gluon densities and saturation momentum

The gluon density in the nucleus is, up to a numerical coefficient, given by the function $h(y, k, b)$ introduced in (7) [3]:

$$\frac{\mathrm{d}[xG(x,k^2,b)]}{\mathrm{d}^2b\mathrm{d}^2k} = \frac{2N_c}{\pi g^2}h(y,k,b), \quad y = \ln\frac{1}{x}. \tag{41}$$

The role of h as the gluon density is clearly illustrated in the factorized forms of the inclusive cross-sections (22) and (23) for pA and AA collisions. In the KT inclusive cross-section for hA collisions the function $h(y, k, b)$ is however substituted by $(1/2)w(y, k, b)$, which can also be considered an effective gluon density taking into account the contribution from the emission vertex. Both densities are well defined for fixed b. As mentioned, at $\bar{y} \geq 1$ they acquire a scaling behavior and depend only on the ratio $k/Q_s(y, b)$ where Q_s is the saturation momentum. In the minimum bias pA collisions and in AB collisions at a fixed impact parameter they are smeared out over the nucleus transverse space. In Fig. 3 we illustrate the gluon densities h and w at $b = 0$ for $A = 180$ and $\bar{y} = 2$, which, with our value for α_s, corresponds to $y \sim 10$. As one observes, both functions have the same form, with a clear maximum at a certain value of k. This value for h is the value for the saturation momentum Q_s [18]. For w the maximum is somewhat shifted towards higher momenta and the value of $(1/2)w$ at the maximum is lower than that for h. As is clear from our formulas for the inclusive cross-sections, these two properties have opposite effects, so that in the end the inclusive cross-sections derived from AGK and introduced by KT as a result are practically equal. In Fig. 4 we show the dependence of the saturation momentum Q_s on b for $A = 180$ and at $\bar{y} = 2$. Its form closely follows the nuclear density $T_A(b)$ reaching $3.8\,\mathrm{GeV}/c$ at the center and dropping to $0.25\,\mathrm{GeV}/c$ and lower at its periphery.

3.2 pA cross-sections

Passing to pA cross-sections we start with the total cross-sections (8). They are shown in Fig. 5 as a function of y for $A = 9, 27, 64, 108$ and 180, divided by $A^{2/3}$ to compare with purely geometric cross-sections. As one observes, the cross-sections become strictly geometric at $\bar{y} \simeq 1.2$. At lower energies they grow faster than $A^{2/3}$, at higher energies they grow much slowlier, approximately as $A^{0.2}$. This can be explained by the role of peripheral parts of the nucleus, whose contribution grows with energy due to the absence of non-linear damping effects and is relatively greater in lighter nuclei.

Inclusive cross-sections were calculated at the overall rapidity $\bar{Y} = 4$, which corresponds to the natural rapidity ~ 20. Inclusive cross-sections corresponding to (14) are

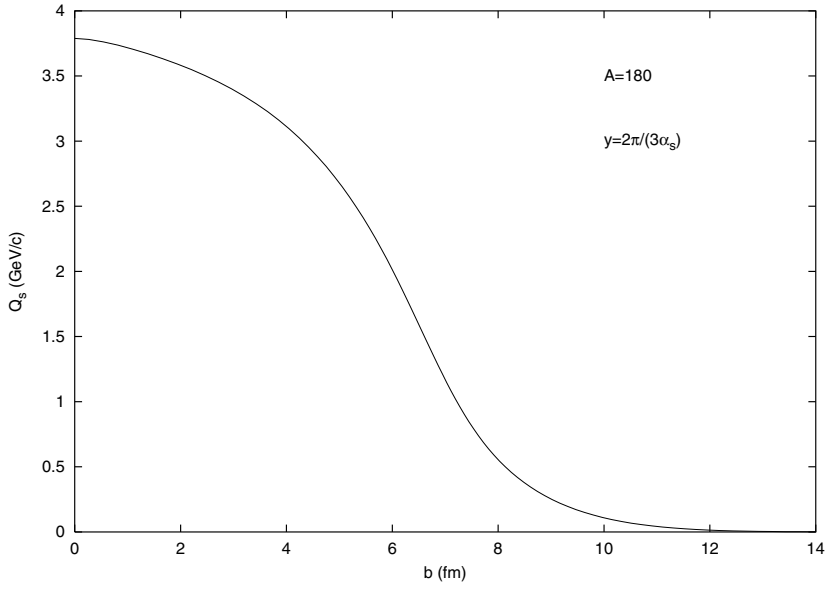

Fig. 4. The saturation momentum Q_s as a function of b for $A = 180$ at $\bar{y} = 2$

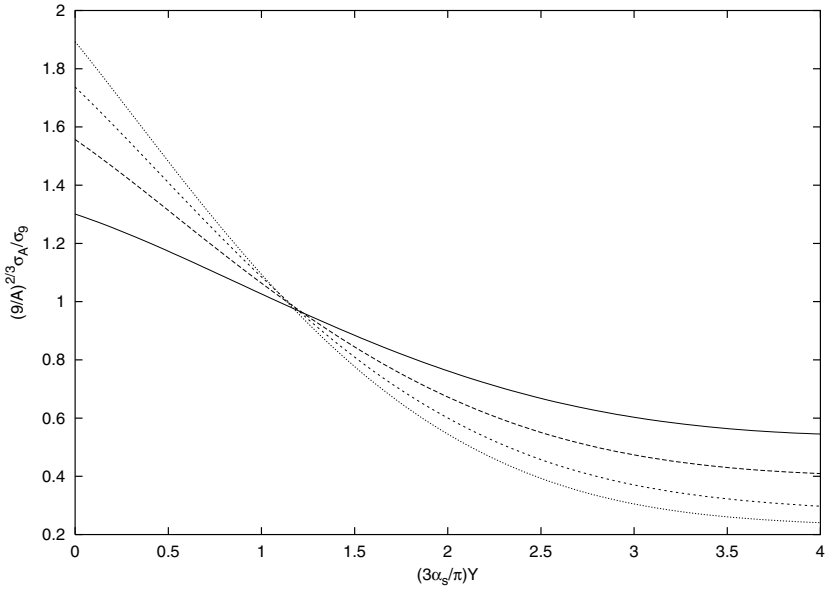

Fig. 5. The total pA cross-sections divided by $A^{2/3}$. Curves from top to bottom on the left correspond to $A = 9, 27, 64, 108$ and 180

shown in Figs. 6–8. Absolute values for the inclusive cross-sections are presented in Fig. 6 for $A = 108$ at central rapidity ($y = Y/2$). At $k < Q_\mathrm{s}$ they are $\propto 1/k^2$, so that the integral factor in (14) is practically constant. At $k > Q_\mathrm{s}$ the cross-sections fall more rapidly. At $k \gg Q_\mathrm{s}$ they behave as $\sim 1/k^{3.1}$. However this asymptotic is only reached at very high nomenta $\sim 10^5$ GeV/c. In Fig. 7 we show the inclusive cross-sections for $A = 108$ at different rapidities relative to the central rapidity. As expected, the cross-sections grow towards the projectile region, since the rapidity of the pure pomeron factor is growing in this region. The A-dependence of the inclusive cross-sections is different at low momenta, below Q_s and high momenta, much larger than Q_s. This is illustrated in Fig. 8, where we plot $(9/A)^{0.745} I_A(k)/I_9(k)$. It is clearly seen that at low momenta the cross-sections are $\propto A^{0.745}$ whereas at high momenta they grow faster with A, approximately as $A^{0.9}$. In any case their growth with A is damped as compared with naive probabilistic expectations which predict them to be $\propto A$.

Passing to the determination of multiplicities one has to observe a certain care because of the properties of the perturbative QCD solution in the leading approximation embodied in (14) and (15). As follows from these formulas inclusive cross-sections blow up at $k^2 \to 0$ independently of the rapidity y. So the corresponding total multiplicity diverges logarithmically. However, the physical sense has only emission of jets with high enough transverse momenta. Thus one has to cut the spectrum from below by some k_min which separates the spectrum of jets proper from soft gluons which are not related to jets. Inevitably the multiplicity of the jets thus defined depends on the chosen value of k_min. We have chosen $k_\mathrm{min} = 2\,\mathrm{GeV}/c$. In Fig. 9 we show multiplicities at $\bar{Y} = 2$ divided by $A^{2/3}$ as a function of the rapidity y. One observes that on the whole the multiplicities

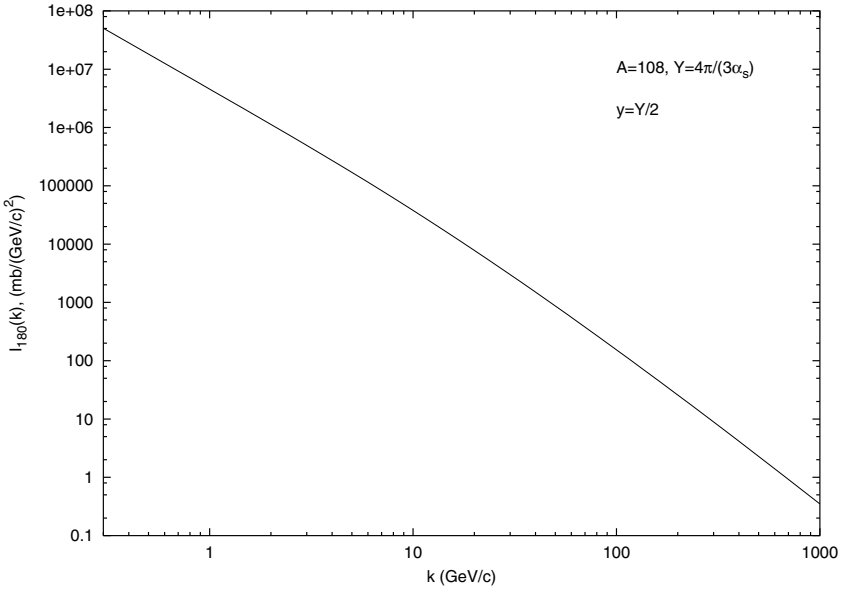

Fig. 6. Inclusive pA cross-sections for $A = 108$ at $\bar{Y} = 4$ and $y = Y/2$

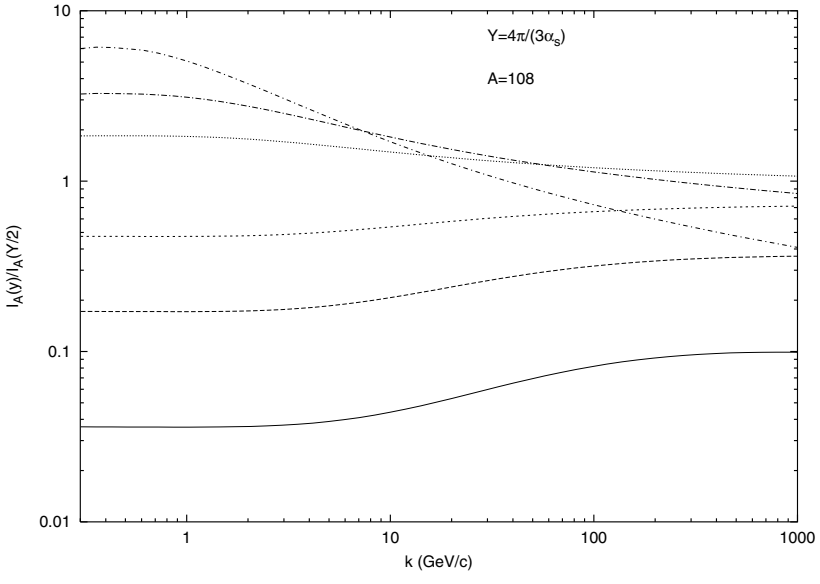

Fig. 7. Inclusive pA cross-sections for $A = 108$ at $\bar{Y} = 4$ and different y relative to $y = Y/2$. Curves from top to bottom correspond to $y/Y = 1/8, 1/4, 3/8, 5/8, 3/4$ and $7/8$

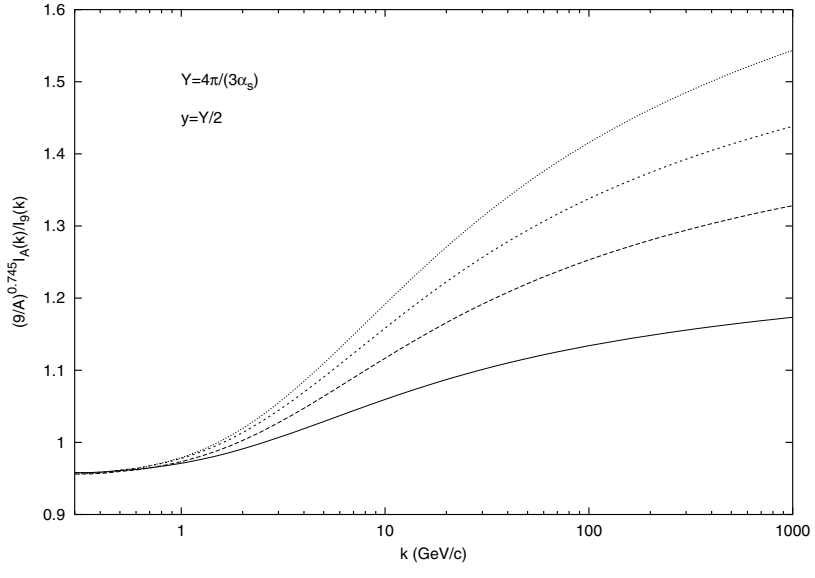

Fig. 8. The A-dependence of inclusive pA cross-sections at $\bar{Y} = 4$ and $y = Y/2$. Curves from bottom to top on the right correspond to $A = 27, 64, 108$ and 180

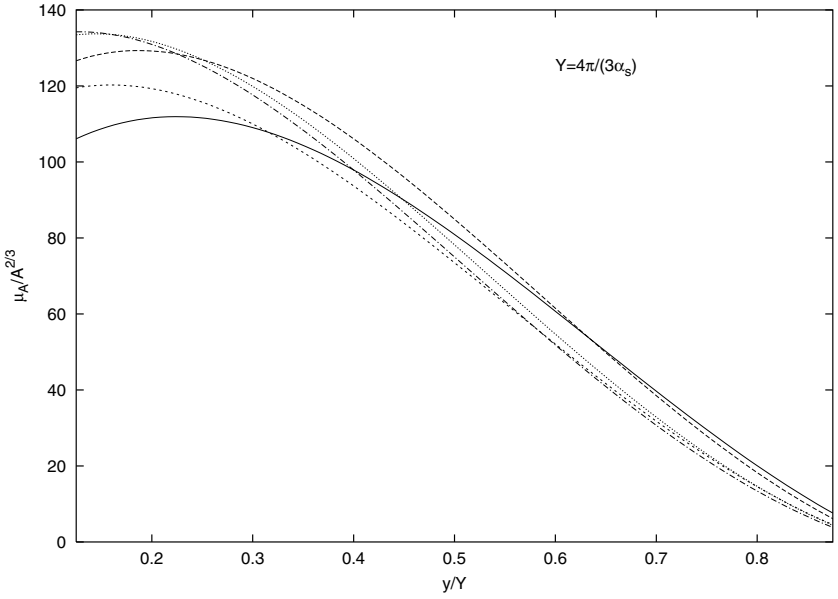

Fig. 9. pA multiplicities at $\bar{Y} = 4$, divided by $A^{2/3}$. Curves from top to bottom on the right correspond to $A = 9, 27, 64, 108$ and 180

are roughly $\propto A^{2/3}$. They diminish with y, except at very small y, which is natural, since the non-linear damping of the gluon density grows as one goes up along the fans.

Finally we pass to the cross-sections obtained with the KT formula (18). In Fig. 10 we show the ratios of these cross-sections to the ones defined by the AGK rules, (14), for $\bar{Y} = 4$ and $y = Y/4, Y/2$ and $(3/4)Y$. These ratios turn to unity at k above Q_s, as discussed in the end of the preceding section. Below Q_s the ratios are in the region $0.72 \div 0.87$ with little dependence on A. Some dependence which is left can be explained by the fact that for the BFKL pomeron attached to the projectile the scaling regime is not valid and that for very peripheral parts of the nucleus it can only be reached at rapidities well above the considered ones. Due to this very simple relation between the two cross-sections, all conclusions about the A-dependence drawn for the AGK cross-section (14) remain valid also for the KT cross-section (18).

3.3 AA collisions

As mentioned, we only considered central collisions of identical nuclei ($A = B$ and $b = 0$). The inclusive cross-sections obtained from the AGK rules (see (15)) are shown in Figs. 11–13. Figure 11 presents absolute values for the inclusive cross-sections for $A = 108$ at center rapidity and different overall energies corresponding to $\bar{Y} = 2, 4$ and 8. As for pA collisions, at $k < Q_\mathrm{s}$ their behavior is totally determined by the $1/k^2$ factor in (19), the integral factor being practically independent of k. At very high momenta $I_A(Y, y = Y/2, k) \sim 1/k^{p(y)}$ with power $p(y)$ diminishing with energy. From our calculations we find that $p(y) \simeq 3.3$, 3.0 and 2.7 at $\bar{y} = 2$, 4 and 8 respectively. At infinite energies p seems to tend to 2 in correspondence with $Q_\mathrm{s} \to \infty$. To see the dependence on the rapidity y of produced particles, in Fig. 12 we show the cross-sections at different y for $A = 108$ and the overall rapidity $\bar{Y} = 4$. As expected the cross-sections steadily diminish towards the edges, their form not changing seriously. The A-dependence of the cross-sections is illustrated in Fig. 13 where we show the ratio $(9/A)I_A/I_9(k)$ at mid-rapidity for the overall rapidity $\bar{Y} = 4$. As in the pA case, we observe scaling at momenta below Q_s, which tells us that at such k the cross-sections are $\propto A$ with a good precision. At momenta higher than Q_s they grow with A faster. In our calculations we found that at very high momenta the cross-sections grow as $\propto A^{1.1}$, that is much slowlier than $A^{4/3}$ as expected from probabilistic considerations.

Multiplicities $\mu(y)$ are obtained in AA case from the integration of $I_A(y, k)$ over $k \geq k_\mathrm{min} = 2\,\mathrm{GeV}/c$. In Fig. 14 we show them divided by A for different y at the overall rapidity $\bar{Y} = 4$. We see approximate scaling. However the multiplicities in fact grow somewhat faster than A, which is explained by the contribution of the high momentum tail of the spectra. The change of the form of the y-dependence with the overall energy is illustrated in Fig. 15 where we plot $\mu(y)/\mu(Y/2)$ at $\bar{Y} = 2, 4$ and 8 for $A = 180$. One observes that the peak of the multiplicity at mid-rapidity becomes narrower with the growth of energy.

All cross-sections discussed so far were obtained from the expression (15) derived from the AGK rules. We finally discuss the AA cross-sections described by the KT formula (19). As for the pA case we present the ratios of the latter cross-sections to the AGK cross-sections in Fig. 16.

These ratios do not practically depend on A, so we show them for $A = 180$ and different y at the total energy corresponding to $\bar{Y} = 4$. Their behavior is quite similar to the pA case. At momenta below Q_s the KT cross-sections are somewhat smaller than the AGK ones. Their ratios grow with y from ~ 0.6 at $\bar{y} = 0.5$ to ~ 0.8 at $\bar{y} = 2$ (mid-rapidity). Note that at $\bar{y} = 0.5$ the lower part of the gluon distribution is still quite far from its asymptotic (scaling) form. So the values for the cross-section at this rapidity preserve a good deal of their dependence on the initial conditions and are not characteristic for the fully evolved

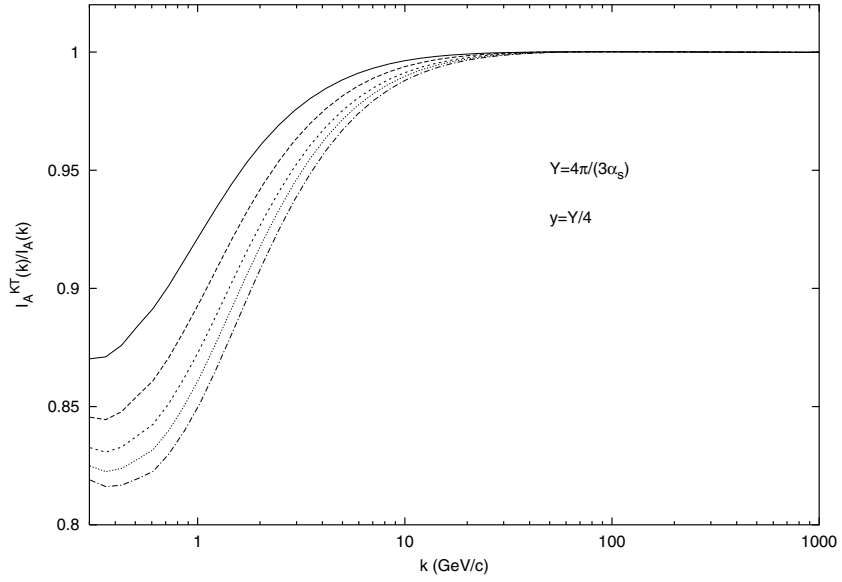

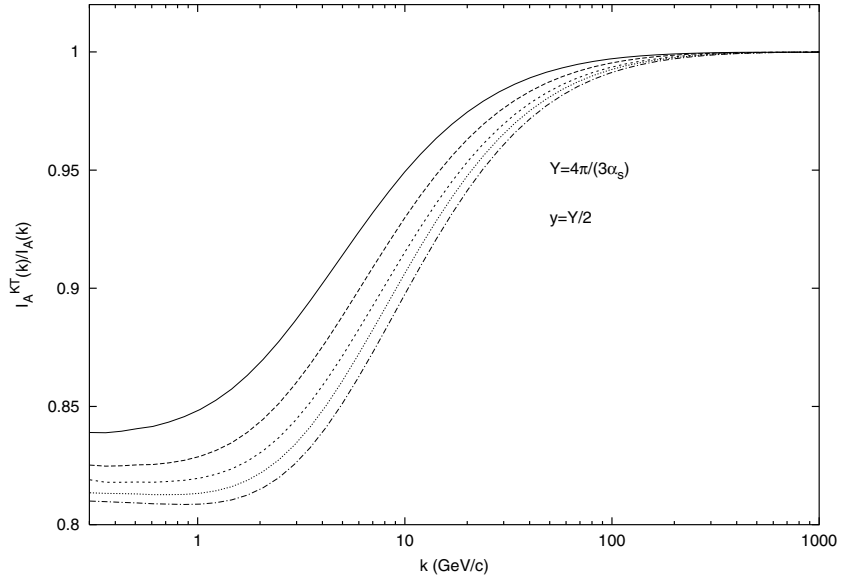

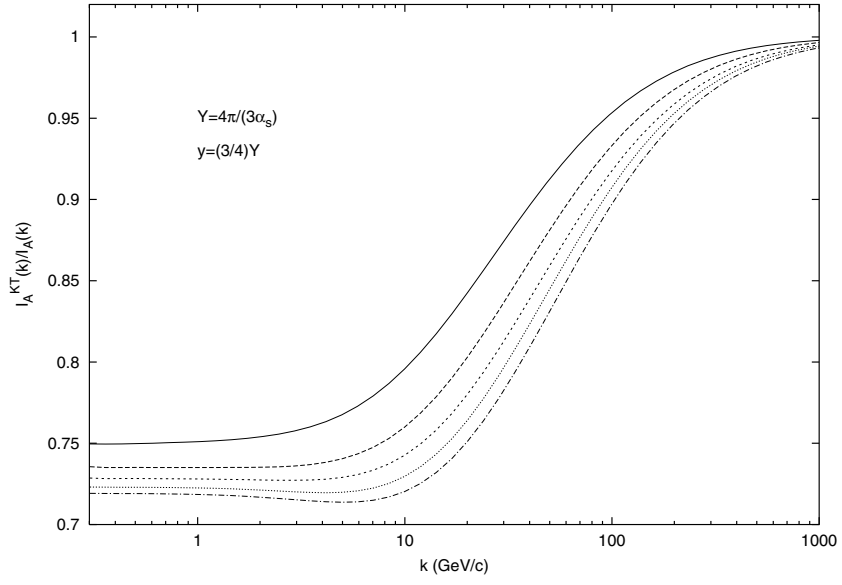

Fig. 10. Ratios of the KT inclusive pA cross-sections, (18), to the ones found from the AGK rules, (14) at $\bar{Y} = 4$. Curves from top to bottom refer to $A = 9, 27, 64, 108$ and 180

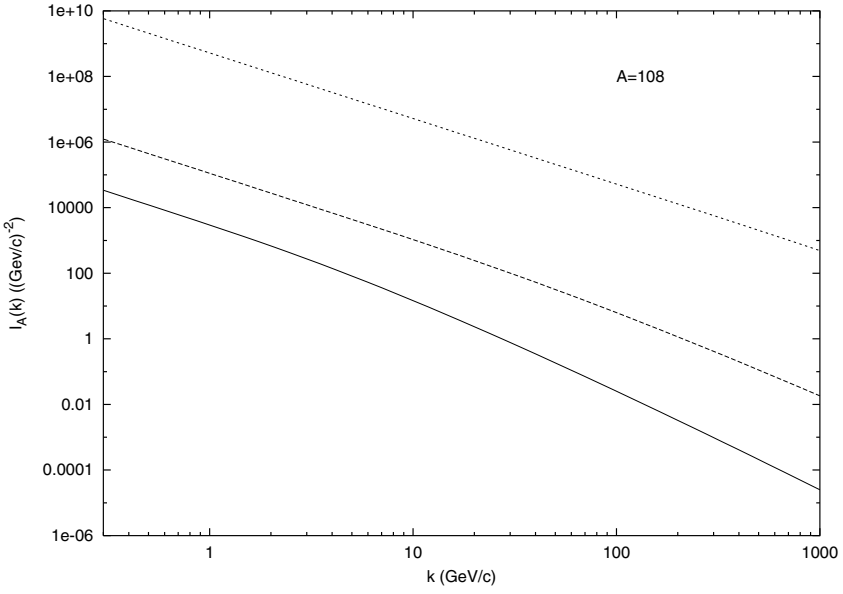

Fig. 11. AA inclusive cross-section at mid-rapidity ($y = Y/2$) for $A = 180$ Curves from top to bottom correspond to the overall rapidities $\bar{Y} = 8, 4$ and 2

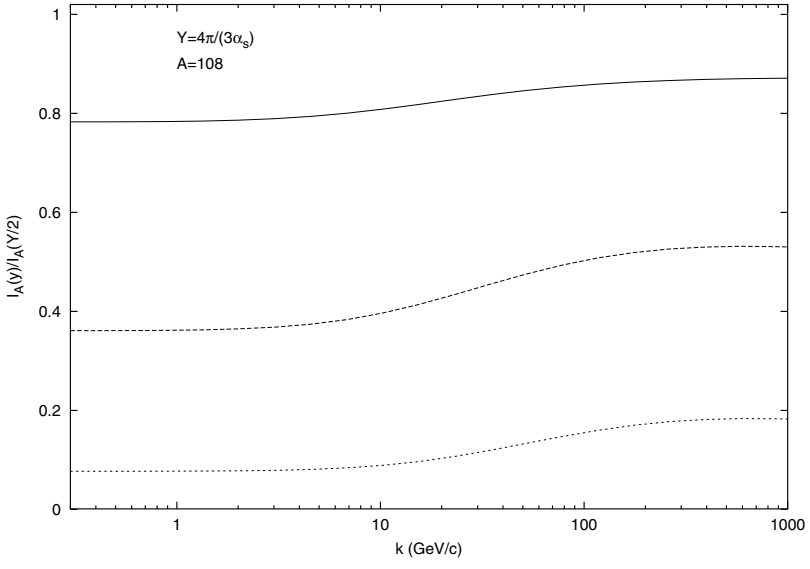

Fig. 12. AA inclusive cross-setions at different y for $A = 180$ and $\bar{Y} = 4$ relative to mid-rapidity $y = Y/2$. Curves from top to bottom correspond to $y = (3/8)Y, (1/2)Y$ and $(1/8)Y$

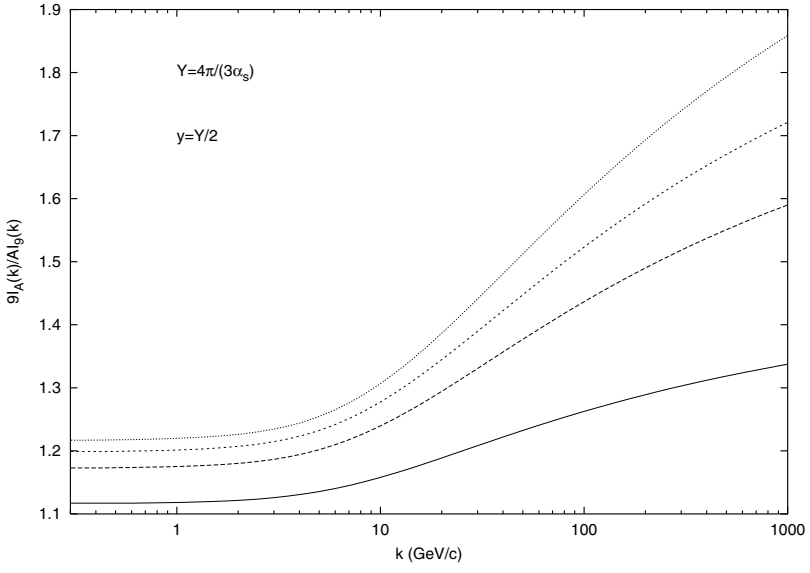

Fig. 13. The ratios $(9/A)I_A(k)/I_9(k)$ for AA collisions at $\bar{Y} = 4$ and $y = Y/2$. Curves from bottom to top correspond to $A = 27, 64, 108$ and 180

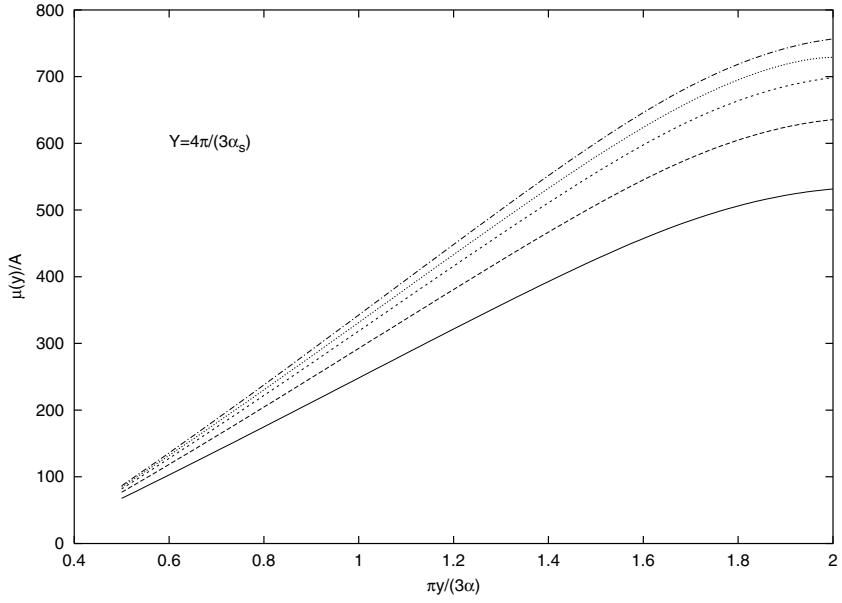

Fig. 14. AA multiplicities divided by A at different y for the overall rapidity $\bar{Y} = 4$. Curves from bottom to top correspond to $A = 9, 27, 64, 108$ and 180

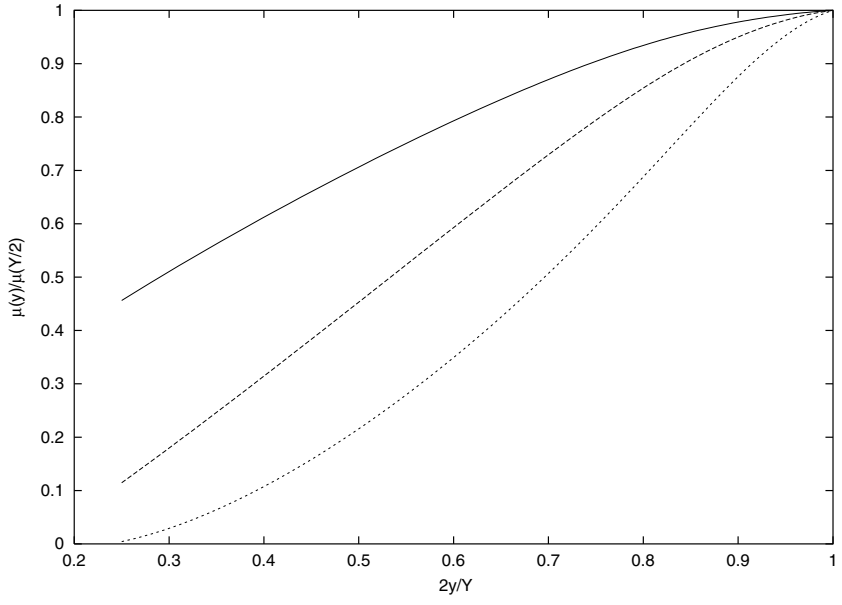

Fig. 15. The form of AA multiplicities at different energies for $A = 180$. Curves from top to bottom correspond to $\bar{Y} = 2, 4$ and 8

dynamics of nuclear interaction. At momenta much higher than Q_s all ratios tend to unity, so that the KT recipe gives the same results as the AGK one.

4 Conclusions

We have calculated the inclusive cross-sections and multiplicities for gluon production in proton–nucleus collisions and nucleus–nucleus central collisions in the perturbative QCD hard pomeron approach with a large number of colors. Realistic nuclear densities were employed to account for the peripheral parts of the nuclei, whose contribution rapidly grows with energy due to the smallness of the unitarizing non-linear effects. In contrast to the structure functions, hadronic processes required the introduction of a new parameter in the model, the value of the strong coupling cosntant at very small energies corresponding to the proton structure.

The form of the cross-sections is found to be determined by the value of the saturation momentum Q_s, which depends on the rapidity and nuclear density. At momenta much lower than Q_s the spectrum is proportional to $1/k^2$. Its A-dependence is close to $A^{0.7}$ for pA collisions and linear for AA collisions at $b = 0$. At momenta much higher than Q_s the spectrum is found to fall approximately as $1/k^{2.7\div3.3}$ with the A-dependence as $\sim A^{0.9}$ for pA and $\sim A^{1.1}$ for AA collisions. The multiplicities are found to be proportional to $A^{0.7}$ for pA and A for AA collisions. Their peak at mid-rapidity for AA collisions becomes more pronounced with the growth of energy.

We also compared two different forms for the inclusive cross-section, which follow from the AGK rules or the dipole picture. The difference between their predictions was

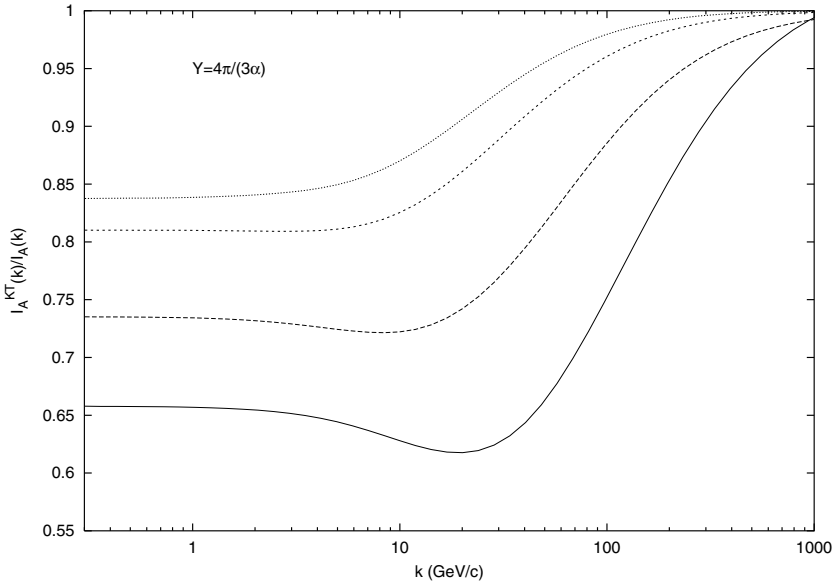

Fig. 16. Ratios of the KT inclusive AA cross-sections, (19), to the ones found from the AGK rules, (15), at $\bar{Y} = 4$ for $A = 180$. Curves from bottom to top refer to $y = (1/8)Y, (1/4)Y, (3/8)Y$ and $(1/2)Y$ (mid-rapidity)

found to be absent for values of momenta larger than Q_s. At momenta smaller than Q_s the difference reduces to a universal constant factor: the dipole cross-sections are just $\sim 0.7 \div 0.8$ of the AGK cross-sections. With the growth of energy this factor slowly grows towards unity, so that it is not excluded that at infinite Y the two cross-sections totally coincide at all values of momenta. All our conclusions about the energy, momentum and A-dependence are equally valid for both forms of the inclusive cross-sections.

As mentioned in the Introduction a few more phenomenological studies of the gluon production in nucleus–nucleus collisions were recently made in the classical approximation to the color-glass condensate model [10] and in the saturation model of [11]. In both studies quantum evolution was neglected, so that scaling with the saturation momentum Q_s was postulated rather than derived. The saturation momentum thus appeared as an external parameter, whose A- and Y-dependence were chosen on general grounds and whose values were fitted to the experimental data at RHIC. In both models the multiplicities turned out to be proportional to the number of participants (modulo logarithmic dependence on A). This agrees with our results. However the form of the inclusive distributions in momenta found in [10] is different from ours. Its behavior both at small k ($\sim 1/\sqrt{k^2+m^2}$ with $m = 0.0358 Q_s$) and at large k ($\sim 1/k^4$) disagrees with the form of the spectrum we have found. For realistic nuclei the spectrum was calculated in [10] only up to $6 \div 7\,\mathrm{GeV}/c$, so it is not possible to see if any change in its A-behavior will occur at higher momenta. The value of the saturation momentum and the speed of its growth with rapidity which we have found from the QCD pomeron model with full quantum evolution are larger than the fitted values in both [10] and [11]. This is no wonder in view of a very high value of the BFKL intercept in the leading approximation which is obtained with the value for the strong coupling constant at present energies. From the phenomenological point of view this is the main drawback of the BFKL theory. To cure it one possibly has to include higher orders of the perturbation expansion and the running coupling constant. Although some work in this direction has been done for linear evolution [19], no attempts to generalize this to non-linear evolution in some rigour has been made yet. As it stands, the model can pretend to describe the data at energies considerably above the presently achieved. One may hope that future data from experiments at LHC will be more suitable for the theoretical analysis in the framework of the model. Of course, the use of a fixed coupling constant in the model casts certain doubts on its applications. However, with a modest change in rapidity the corresponding change of the running coupling is also very modest. So one expects the effects of the running to be pronounced only at very large rapidity distances. Calculations in which the running of the coupling was introduced in some primitive manner have shown that even at superhigh energies the resulting change is not dramatic [20]. So we remain optimistic about the application of the model to the experimental results in the several-TeV region.

Acknowledgements. The author is deeply indebted to Yu. Kovchegov for a constructive discussion and valuable comments and to N. Armesto and B. Vlahovic for their interest in this work. This work has been supported by a NATO Grant PST.CLG.980287.

References

1. E.A. Kuraev, L.N. Lipatov, V.S. Fadin, Sov. Phys. JETP **45**, 199 (1977); Ya.Ya. Balitsky, L.N. Lipatov, Sov. J. Nucl. Phys. **28**, 22 (1978)
2. Yu.V. Kovchegov, Phys. Rev. D **60**, 034008 (1999); D **61**, 074018 (2000)
3. M.A. Braun, Eur. Phys. J. C **16**, 337 (2000)
4. M.A. Braun, Phys. Lett. B **483**, 115 (2000)
5. M.A. Braun, Eur. Phys. J. C **33**, 113 (2004)
6. M.A. Braun, Phys. Lett. B **483**, 105 (2000)
7. V.A. Abramovsky, V.N. Gribov, O.V. Kancheli, Sov. J. Nucl. Phys. **18**, 308 (1974)

8. J.L. Albacete, N. Armesto, A. Kovner, C.A. Salgado, U.A. Wiedemann, Phys. Rev. Lett. **92**, 082001 (2004)
9. D. Kharzeev, Yu. Kovchegov, K. Tuchin, hep-ph/0405045
10. A. Krasnitz, Y. Nara, R. Venugopalan, Phys. Rev. Lett. **87**, 192302 (2001); Nucl. Phys. A **717**, 268 (2003)
11. D. Kharzeev, M. Nardi, Phys. Lett. B **507**, 121 (2001); D. Kharzeev, E. Levin, Phys. Lett. B **523**, 79 (2001)
12. Yu. Kovchegov, K. Tuchin, Phys. Rev. D **65**, 074026 (2002)
13. L.D. McLerran, R. Venugopalan, Phys. Rev. D **49**, 2233, 3352 (1994); D **50**, 2225 (1994); E.G. Ferreiro, E. Iancu, A. Leonidov, L.D. McLerran, Nucl. Phys. A **703**, 489 (2002)
14. M.A. Braun, hep-ph/0407346, to be published in Phys. Lett. B
15. K. Golec-Biernat, M. Wuesthoff, Phys. Rev. D **59**, 014017 (1999); D **60**, 114023 (2000)
16. M. Ciafaloni et al., Nucl. Phys. B **98**, 493 (1975)
17. J. Bartels, M. Wuesthoff, Z. Physik, C **66**, 157 (1995)
18. N. Armesto, M.A. Braun, Eur. Phys. J. C **20**, 517 (2001)
19. V.S. Fadin, L.N. Lipatov, Phys. Lett. B **429**, 127 (1998); G. Camici, M. Ciafaloni, Phys. Lett. B **412**, 396 (1998); B **430**, 349 (1998)
20. M.A. Braun, Phys. Lett. B **576**, 115 (2003)